

Hydrogen selectivity and carbon behavior during gasoline steam reforming over nano- Al_2O_3 catalysts

Dalia R. Abd El-Hafiz · Mohamed A. Ebiad ·
Radwa A. El-salamony

Received: 2 March 2014 / Accepted: 21 June 2014 / Published online: 3 August 2014
© The Author(s) 2014. This article is published with open access at Springerlink.com

Abstract In this work, the influence of metal type (Ni and Co) and preparation method (co-precipitation and impregnation) on catalytic gasoline steam reforming (CGSR) using nano- Al_2O_3 support were studied at different reaction temperature (500–800 °C). The structure and surface properties of fresh and spent catalysts were tested by different characterization tools such as TGA, TPR, XRD, HRTEM, BET surface areas and Raman spectroscopy. Results show that product distribution is dependent on both preparation method and metal type. Co/ Al_2O_3 is the most selective catalyst for hydrogen production from GSR reaction; H_2 selectivity reached 70 % over this catalyst at 800 °C. While, when considering hydrogen production and carbon deposition in the meantime, Ni/ Al_2O_3 is the best one because of the generation of non-deactivating carbon on its surface. CO conversion represented as $\text{CO}_2/(\text{CO} + \text{CO}_2)$ is an indication of the WGS reaction, over all of the prepared catalysts, WGS reaction was preferred at low temperature. On the other hand, we can show that Ni catalysts favor WGS reaction more than that of co catalyst. Moreover, a higher thermal stability and graphitization degree of deposit carbon were obtained on Ni- Al_2O_3 and Co/ Al_2O_3 .

Keywords Gasoline reforming · Carbon deposition · Hydrogen production · Nano- Al_2O_3 catalysts

Introduction

Nowadays, the automotive industry pays great attention to catalytic reforming of gasoline (CRG) to produce

hydrogen, owing to the existing infrastructure and high power density of gasoline. This hydrogen can be transformed cleanly and efficiently into electricity using fuel cells. CRG has two advantages when used as fuel: first, the higher energy efficiency with respect to the use of internal combustion engine. Second, it has an environmental impact by eliminating the pollutant emissions such as NO_x produced from internal combustion engines.

The main catalytic reactions for hydrogen production from petroleum fuels [1, 2] are steam reforming, partial oxidation, and auto-thermal reforming. Among those methods, catalytic steam reforming (CSR) shows the highest conversion to H_2 [3, 4]. In order to achieve high H_2 selectivity on a metallic catalyst for the CSR, the catalysts should have a high C–C bond breaking rate and a low methanation reaction rate. Mono-metallic noble catalysts, such as Pt, depending on the support could demonstrate high H_2 selectivity. However, the high cost of Pt makes it economically infeasible to use [5]. The commercial catalysts used in steam reforming are Ni/ Al_2O_3 and Ni/MgO [6, 7]. According to the literature [8–10] Ni is a potential catalyst for the steam reforming reactions because it has high rate of C–C bond breakage, good water gas shift activity, and moderate methanation reaction capacity.

High specific surface area, homogeneous dispersion of metals, design of meso-pore structure, control of metal–support interaction, and also preparation of catalysts in nano-form are other important factors showing better catalytic activity and stability in steam reforming reaction [11]. Nano-sized catalysts are prepared either by impregnation or co-precipitation of metal with the support [12].

However, coking is a major problem associated with reforming of heavy hydrocarbon fuels such as gasoline over different catalysts. It is well known that the origin of carbon deposit could be different using different catalysts

D. R. Abd El-Hafiz (✉) · M. A. Ebiad · R. A. El-salamony
Egyptian Petroleum Research Institute, Cairo 11727, Egypt
e-mail: dalia_epri@yahoo.com

[13]. There are several studies that reported the better stability and suppression of carbon deposition when using cobalt, compared with nickel [14, 15].

Therefore, the aim of the present work was to study the performance of nano-sized Ni- and Co- Al_2O_3 prepared by different methods as catalysts in gasoline steam reforming reaction. The detailed study of the amount and type of carbon deposition will be carried out.

Experimental

Catalyst preparation

Impregnation method

First, nano-sized porous gamma-alumina ($\gamma\text{-Al}_2\text{O}_3$) was prepared by control precipitation method [16] in which two solutions of ammonium bicarbonate [$(\text{NH}_4\text{HCO}_3, 98 \%)$ (Merck)] and (0.066 M) aluminium nitrate [$(\text{Al}(\text{NO}_3)_3 \cdot 9\text{H}_2\text{O}, 95 \%)$ (Merck)] were added dropwise to deionized water. The pH of $\text{Al}(\text{OH})_3$ gel was adjusted at ~ 10 using NaOH solution. The precipitate was aged at 70°C for 3 h, filtered, and washed with deionized water, dried, and then calcined in air at 550°C for 5 h to produce $\gamma\text{-Al}_2\text{O}_3$ powders. Co/ Al_2O_3 and Ni/ Al_2O_3 samples were prepared by impregnating $\gamma\text{-Al}_2\text{O}_3$ support with aqueous solutions of $\text{Co}(\text{NO}_3)_2 \cdot 6\text{H}_2\text{O}$ or $\text{Ni}(\text{NO}_3)_2 \cdot 6\text{H}_2\text{O}$, respectively, to produce 10 % metal loading. All samples were calcined at 700°C for 5 h.

Co-precipitation method

Likewise of $\gamma\text{-Al}_2\text{O}_3$ preparation method the Ni- Al_2O_3 sample was prepared by a control precipitation method using a mixture of $\text{Al}(\text{NO}_3)_3 \cdot 9\text{H}_2\text{O}$ and (0.066 M) $\text{Ni}(\text{NO}_3)_2 \cdot 6\text{H}_2\text{O}$. The catalysts Co/ Al_2O_3 , Ni/ Al_2O_3 , and Ni- Al_2O_3 are typical as Co/Al, Ni/Al and Ni-Al respectively.

Characterization methods

Thermal gravimetric analysis (TGA) was carried out using SETARAM Labsys TG-DSC16 equipment in the temperature range from room temperature up to $1,000^\circ\text{C}$ under N_2 flow in case in fresh catalysts and O_2 in case of spent one to follow the thermal stability of the prepared catalyst.

X-ray diffraction analysis (XRD) was carried out by Shimadzu XD-1 diffractometer using Cu-target and Ni-filtered radiation, at step size of 0.02° and scan step time 0.4 s. The phase identification was made by comparing to the Joint Committee on Powder Diffraction Standards (JCPDS). The crystallite size of the prepared samples was

determined from the XRD peaks using the Scherrer equation.

Transmission electron microscopy (TEM) and energy dispersive X-ray (EDS) spectroscopy take place using a JEOL 2100F TEM at an accelerating voltage of 200 kV. The samples were sonicated for 30 min in ethanol and then a drop of this solution placed on a carbon coated Cu grid.

The textural properties were determined from the N_2 adsorption-desorption isotherms measured at liquid nitrogen temperature (-196°C) using NOVA2000 gas sorption analyzer (Quantachrome Corporation) system. All of the prepared samples were degassed at 200°C for 17 h in nitrogen atmosphere before measurement to ensure a dry clean surface. The adsorption isotherm was constructed as the volume adsorbed (Vcm^3/g) versus the equilibrium relative pressure P/P_0 .

Temperature programmed reduction (TPR) measurements were carried out to investigate the redox properties (the ease of reducibility of metal oxide) over the resultant materials. The experiments were performed in automatic equipment (Chem BET 3000, Quantachrome). Typically, 100 mg of pre-calcined sample was loaded into a quartz reactor and pretreated by heating under inert atmosphere (20 ml/min nitrogen) at 200°C for 3 h prior to running the TPR experiment and then cooled down to room temperature in N_2 . At that point, the sample was submitted to a constant rate of heat treatment ($10^\circ\text{C}/\text{min}$ up to $1,000^\circ\text{C}$) in a gas flow (80 ml/min) of the mixture hydrogen/nitrogen (5/95 Vol%) as a reducing gas. A thermal conductivity detector (TCD) was employed to monitor the amount of hydrogen consumption.

Raman spectra were carried out at room temperature, using HR UV 800 confocal scanning spectrometer (Horiba Jobin Yvon) equipped with a Peltier-cooled charge-coupled device. The Raman scattering was excited using a 632.81-nm excitation wavelength supplied by an internal He-Ne laser through an Olympus high-stability BXFM confocal microscope. Patterns were recorded in the $50\text{--}1,000\text{ cm}^{-1}$ Raman shift range with a spectral resolution of 0.5 cm^{-1} . Lab SPEC v. 5 software was used for data acquisition and processing.

Catalytic activity

Gasoline steam reforming was carried out at atmospheric pressure in a continuous fixed bed, vertical tubular reactor [17]. 1 g of catalyst diluted with quartz particles (1:1) was used for catalytic tests. Before each run, the catalyst was reduced in hydrogen flow ($20\text{ cm}^3/\text{min}$) at 800°C for 2 h. Water/gasoline mixture (gasoline/ $\text{H}_2\text{O} = 1:8\text{ mol/mol}$) was fed into the evaporator (at 150°C) by a dosing pump (Model RP-G6; FMI, USA) with a flow rate 0.2 ml/min. Nitrogen carrier gas was fed into the evaporator with a flow

rate 40 cm³/min to uniformly carry the steam, and the steam was then fed to the reactor. The reaction temperature varied from 500 to 800 °C.

The products were analyzed by gas chromatography (GC) (Agilent 6890 plus HP, Varian Natural Gas Analyzer type C model CP-3800). Selectivity values were calculated as the mole percentage of products obtained, excluding water; selectivity of product = (mol of product/total mol of H₂ and carbon-containing products in the outlet) × 100.

Results and discussion

Catalyst characterization

Thermal gravimetric analysis

The thermal behavior of the prepared samples was investigated using TGA and DTA from room temperature up to 1,000 °C (Fig. 1). The curve shows an endothermic process and an exothermic one in parallel with two weight loss steps; an endothermic peak from 30 to 400 °C is due to loss of physically adsorbed water and the hydroxyl of the catalyst's surface. A high temperature exothermic peak may be related to the crystallization and/or the weight loss due to components' loss of the catalysts caused by certain reactions occurring at the high temperature [18]. From the whole weight loss process of catalysts, it can be seen that the profiles of Ni/Al₂O₃ and Co/Al₂O₃ are almost the same and that their weight loss is higher than that of Ni–Al₂O₃.

X-ray diffraction analysis

XRD patterns of the prepared catalysts are shown in Fig. 2; generally, the broad features of all diffractograms were ascribed to the prepared nano-structured solids. For Ni–Al₂O₃ catalyst, only high intensity and broad diffraction peaks at $2\theta = 37.7^\circ$, 44.56° and 65.96° of NiAl₂O₄

(JCPDS 00-001-1299) are observed. No Bragg reflections were detected for NiO, which suggests that the co-precipitation method leads to the incorporation of small particle size NiO in Al₂O₃ structure to form the NiAl₂O₄ spinel phase [19].

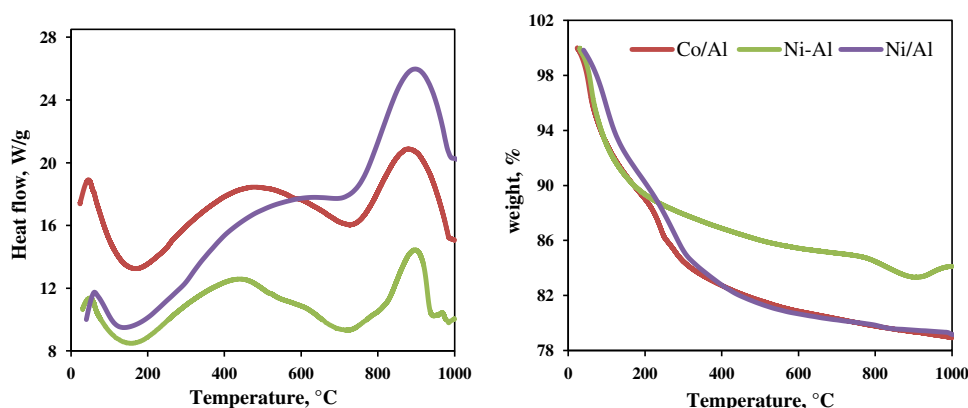
However, XRD pattern of Ni/Al₂O₃ catalyst prepared by impregnation method shows peaks attributed to NiO phase at 2θ 43.29° and 62.77° (JCPDS 00-001-1258) in addition to that for Al₂O₃, which ascribed to the inhomogeneous distribution of the Ni species [19]. Figure 2b shows an enlarged pattern (from 2θ 60° to 70°) to show the difference between Al₂O₃ and NiAl₂O₄ peaks, which were difficult to be distinguished due to its broadening. Moreover, the particle size of NiAl₂O₄ is smaller for Ni–Al₂O₃ (7.2 nm) catalyst than for Ni/Al₂O₃ (8.66 nm) as shown in Table 1.

It is noteworthy that XRD pattern of Co/Al₂O₃ shows different peaks, peaks at 2θ 31.4°, 37° and 59.53° (JCPDS 00-001-1152) were ascribed to cubic Co₃O₄ crystallites [20], in addition to Al₂O₃ peaks. The increase in intensity and sharpness of Al₂O₃ peak at 37° may be due the overlap with the peak assigned to the cubic Co₃O₄ crystallites. No diffraction peak of CoO, cobalt aluminate or other Co species was found as reported by Batista et al. [21]. The average crystal sizes of metals on catalyst surfaces were 17.9 nm for NiO and 26.32 nm for Co₃O₄ in Ni/Al₂O₃ and Co/Al₂O₃, respectively.

Table 1 Textural properties of the prepared samples

Catalyst	BET surface area (m ² /g)	Pore volume (cm ³ /g)	Crystal size (metal oxide) (nm)	Crystal size (support) (nm)
Ni–Al	249	0.57	–	7.2
Ni/Al	91	0.26	17.9	8.7
Co/Al	173	0.67	26.3	9.7

Fig. 1 TGA/DTA profiles of the prepared samples



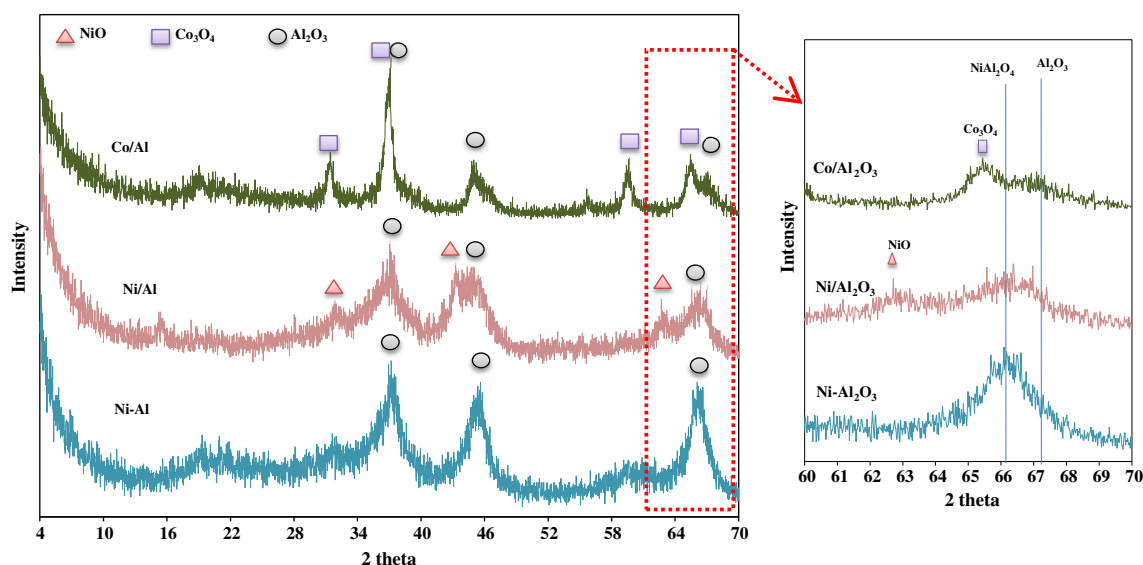


Fig. 2 XRD pattern for the prepared catalyst

High-resolution transmission electron microscopy

The HRTEM photographs obtained from the prepared samples are shown in Fig. 3. Analysis of the photographs for Ni–Al revealed particles with defined dimensions with a slight contraction of the crystal lattice due to partial substitution of Al by Ni, having a grain size ranging from 2 to 4 nm. Although no separate NiO phases were discernible by the XRD of Ni–Al, STEM/EDS elemental mapping (not shown) identified nickel clusters, which indicate that the co-precipitation method leads to incorporation of Ni inside the Al_2O_3 matrix. In Ni/Al and Co/Al systems, two phases are observed, corresponding to the presence of the Al_2O_3 in needle structure, and metal oxide in crystalline structure (indicated by red circle) as expected by XRD data. In the two later catalysts, the mean particle size is estimated to be in the range 10–14 and 18–22 nm, respectively.

Surface areas

The nitrogen adsorption desorption isotherms of the prepared samples are shown in Fig. 4. Ni–Al sample exhibited IV-type isotherm with H2-type hysteresis loop, typical characteristics of mesoporous materials [22] as shown by BJH pore size distributions, and T-plot represented in Fig. 5, which shows the meso-pores material with narrow pore size distributions centered at 4 nm. On the other hand, Ni/Al and Co/Al samples show type II isotherm with H3 hysteresis loop which attributed to slit-shaped pores or plate-like particles with spaces between the parallel plates.

The values of the specific BET surface area and total pore volumes of the prepared samples are listed in Table 1.

Compared with the Ni/ Al_2O_3 prepared by impregnation method, Ni– Al_2O_3 catalyst shows the much higher specific surface area and pore volume, this because in co-precipitation method, Ni species can be uniformly dispersed. Moreover, the inhomogenous distribution of nickel species in Ni/Al catalyst led to blocking of some pores and decrease specific surface area. On the other hand, the impregnation by Co has little effect on the loss of surface area of Al_2O_3 (173 m^2/g), this may be attributed the good dispersion of Co metal on alumina surface.

Temperature programmed reduction (TPR)

Continuing with the idea revealed by Chen et al. [23], that the strong metal–support interaction can effectively suppress the formation of deposit carbon, the TPR results obtain information about the effect of metal type and preparation method on metal–support interaction. The TPR profile for Ni– Al_2O_3 catalyst (Fig. 6), shows only one broad peaks with a maximum at about 850 °C, which mainly due to the reduction of NiO strongly interacted with the support by the formation of amorphous nickel aluminate spinel structure (NiAl_2O_4) as shown from XRD data [19]. This strong metal–support interaction can restrict the agglomeration of active metal and avoid metal sintering during the reaction.

The TPR profile of Ni/ Al_2O_3 catalyst (Fig. 6) shows three distinct regions of temperature, the weakest peak centered at about 304 °C assigned to the reduction of free NiO. The second broad peak at 415 °C was an indication of surface NiO species weakly interacting with the support [24, 25]. The third peak, at about 712 °C, related to the

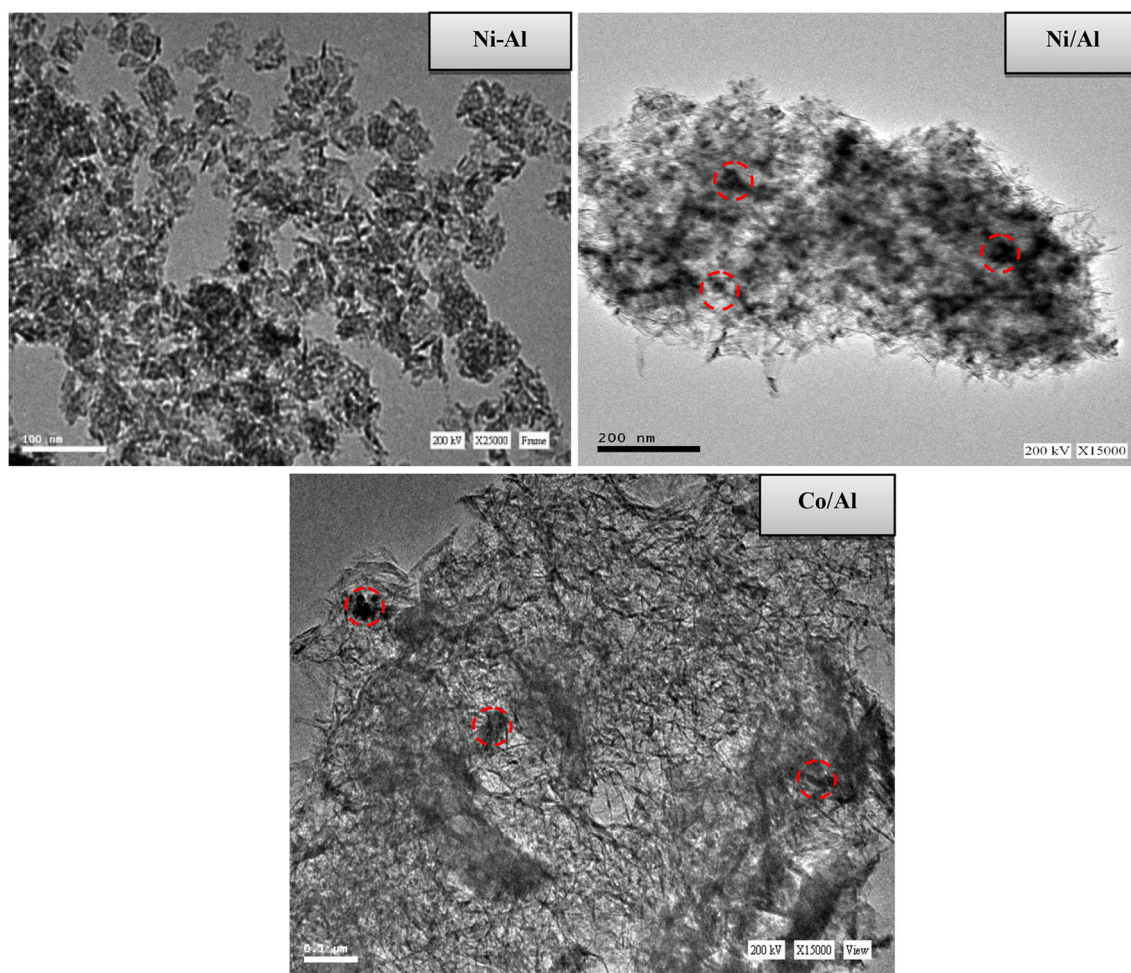


Fig. 3 TEM image of the prepared catalysts

reduction of the stoichiometric and non-stoichiometric nickel aluminate (NiAl_2O_4), which are more difficult to reduce [26]. Those different reduction temperatures were related to the inhomogeneous distribution of the Ni species in the Al_2O_3 support as confirmed by XRD data. So, the catalyst prepared by co-precipitation method shows good Ni dispersion and difficult reduction degree than that prepared by impregnation method.

On the other hand, the TPR profile for $\text{Co}/\text{Al}_2\text{O}_3$ catalysts shows two H_2 consumption peaks, reflecting a two-step reduction process ($\text{Co}_3\text{O}_4 \rightarrow \text{CoO} \rightarrow \text{Co}^0$), as previously described by Jacobs et al. [27]. The reduction of Co_3O_4 to CoO is achieved at 440 °C, and the reduction of CoO to Co^0 occurs around 700 °C (Fig. 2a) [28]. Another small peak at about 840 °C may be due to the small amount of Co species that incorporated (strongly interacted) in the Al_2O_3 structure.

Catalytic activity

Gasoline conversions and product selectivities for steam reforming on the three alumina catalysts are summarized in

Table 2. The gasoline used in this work was desulfurized gasoline (~ 5 ppm sulfur). The main products of gasoline steam reforming are H_2 , CH_4 , CO , CO_2 , C_2H_4 , C_2H_6 , C_3H_8 , C_4H_{10} , C_5H_{12} , and other heavy ends. Several reactions can occur during gasoline steam reforming depending on the reaction conditions [29, 30]; those reactions could be steam reforming reaction (reaction 1), water gas shift reaction (reaction 2), Methanation of CO and CO_2 (reactions 3, 4) and steam reforming of methane (reverse of reaction 3).

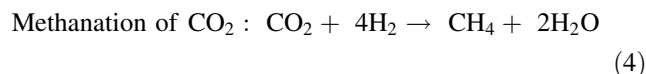
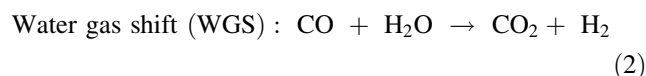
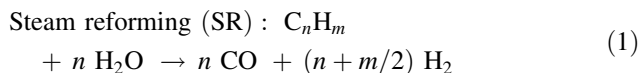


Figure 7 shows that the higher carbon product (heavy ends) overall reaction temperature is lower on $\text{Co}/\text{Al}_2\text{O}_3$

Fig. 4 Nitrogen adsorption–desorption isotherms of the prepared samples

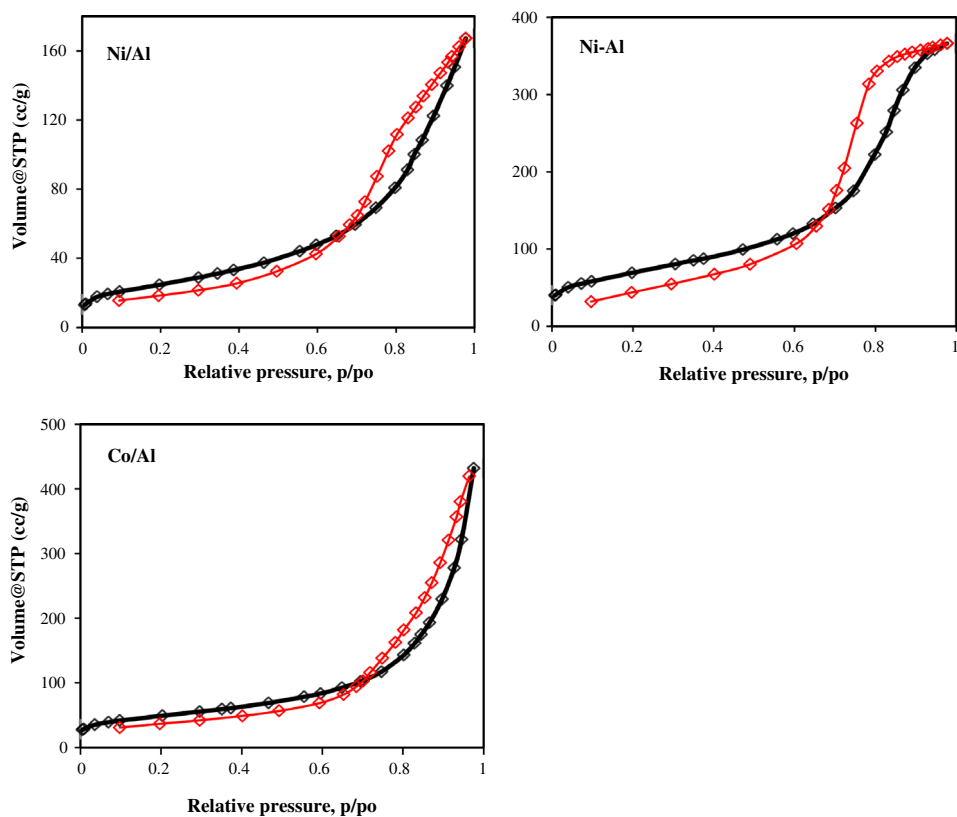
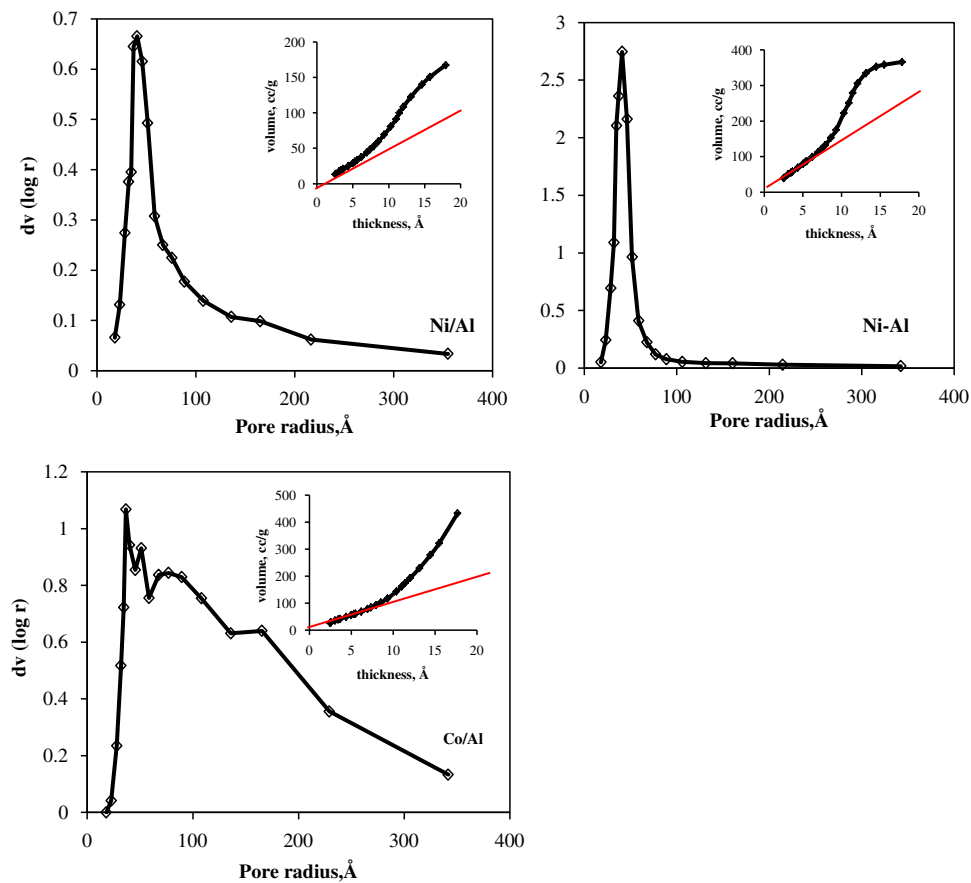


Fig. 5 Pore size distributions and T-plots of the prepared samples



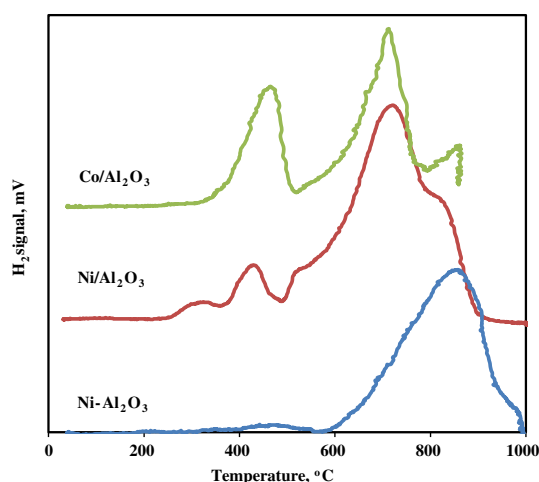


Fig. 6 TPR pattern of the prepared catalysts

than on Ni–Al₂O₃ than Ni/Al₂O₃, which indicates the higher catalytic activity of Co/Al₂O₃ catalyst in gasoline reforming at lower reaction temperature. The higher catalytic activity of Ni–Al₂O₃ than that of Ni/Al₂O₃ may be attributed to the highly homogeneous dispersion and small particle sizes of Ni species in case of catalyst prepared by co-precipitation method, which enhances the reaction efficiency in gasoline reforming.

The product distribution as a function of temperature on all catalysts is compared in Fig. 8. Generally, hydrogen and methane are the major products, while the CO and CO₂ exhibited the lowest selectivity.

The selectivity to H₂ increases as the temperature increases over all catalyst to reach maximum value of 69.88 % at 800 °C over a Co/Al catalyst. Therefore, it is effective to enhance the selectivity to H₂ using Co instead

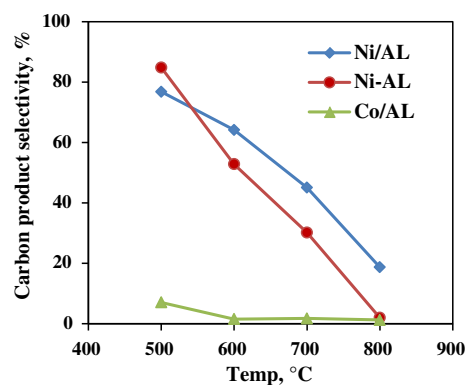


Fig. 7 Selectivity to carbon produced

of Ni as catalyst for gasoline steam reforming. Moreover, the Ni–Al₂O₃ catalyst is more selective to H₂ than Ni/Al₂O₃ catalyst owing to the good Ni dispersion resulted from co-precipitation method as shown by XRD data. So, we can clearly find that the product distribution of steam reforming of gasoline is dependent on both preparation method and metal type.

Figure 9 shows the value of H₂ + CO over the prepared catalysts at all temperature ranges; from this figure we can show that the steam reforming reaction is favored over a Co/Al₂O₃ catalyst than the other catalysts.

Comparing the CH₄ and the CO₂ formation during GSR reaction over different catalysts we can conclude that the reaction mechanism are different over Ni catalysts than that over Co one. From Fig. 10, Co/Al is the most selective catalyst to methane production at lower reaction temperature, while, as the temperature increase the selectivity to methane decrease to reach the lower value 10.15 % at 800 °C. This conduct with low amount

Table 2 Product distribution from GSR

Temp (°C)	Product selectivity (mol %)											
	Ni–Al ₂ O ₃				Ni/Al ₂ O ₃				Co/Al ₂ O ₃			
	500	600	700	800	500	600	700	800	500	600	700	800
Hydrogen	0.82	15.24	20.28	49.75	10.82	13.11	19.22	36.48	23.64	29.58	44.40	69.88
Methane	8.16	29.54	48.55	45.25	9.16	17.03	30.97	37.09	65.44	67.29	39.85	10.15
CO	3.82	1.79	0.71	2.53	1.85	0.84	1.87	6.18	2.72	1.25	13.03	18.14
CO ₂	2.35	0.57	0.30	0.50	1.38	4.86	2.89	1.57	1.14	0.33	0.97	0.59
Ethane	2.78	7.68	4.56	0.43	3.07	3.99	2.65	0.86	0.03	0.01	0.00	0.01
Ethylene	3.79	14.90	18.49	0.88	3.74	11.06	22.69	9.75	0.01	0.01	0.00	0.01
Propane	4.29	12.28	4.12	0.08	5.04	9.15	9.45	1.26	0.02	0.01	0.00	0.02
<i>i</i> -Butane	3.15	0.19	0.02	0.05	2.92	0.24	0.34	1.09	0.04	0.01	0.01	0.00
<i>n</i> -Butane	1.39	6.78	1.41	0.04	5.63	7.93	5.97	1.47	0.14	0.06	0.08	0.04
<i>i</i> -pentane	24.98	3.21	0.29	0.05	0.65	12.27	1.47	1.11	0.09	0.03	0.02	0.12
<i>n</i> -Pentane	8.40	1.34	0.13	0.02	15.79	4.71	0.62	0.59	0.06	0.02	0.01	0.06
Hexane and heavy end	36.07	6.48	1.15	0.42	39.97	14.80	1.85	2.54	6.67	1.41	1.62	0.98

Fig. 8 Product distribution of gasoline steam reforming over the prepared catalysts

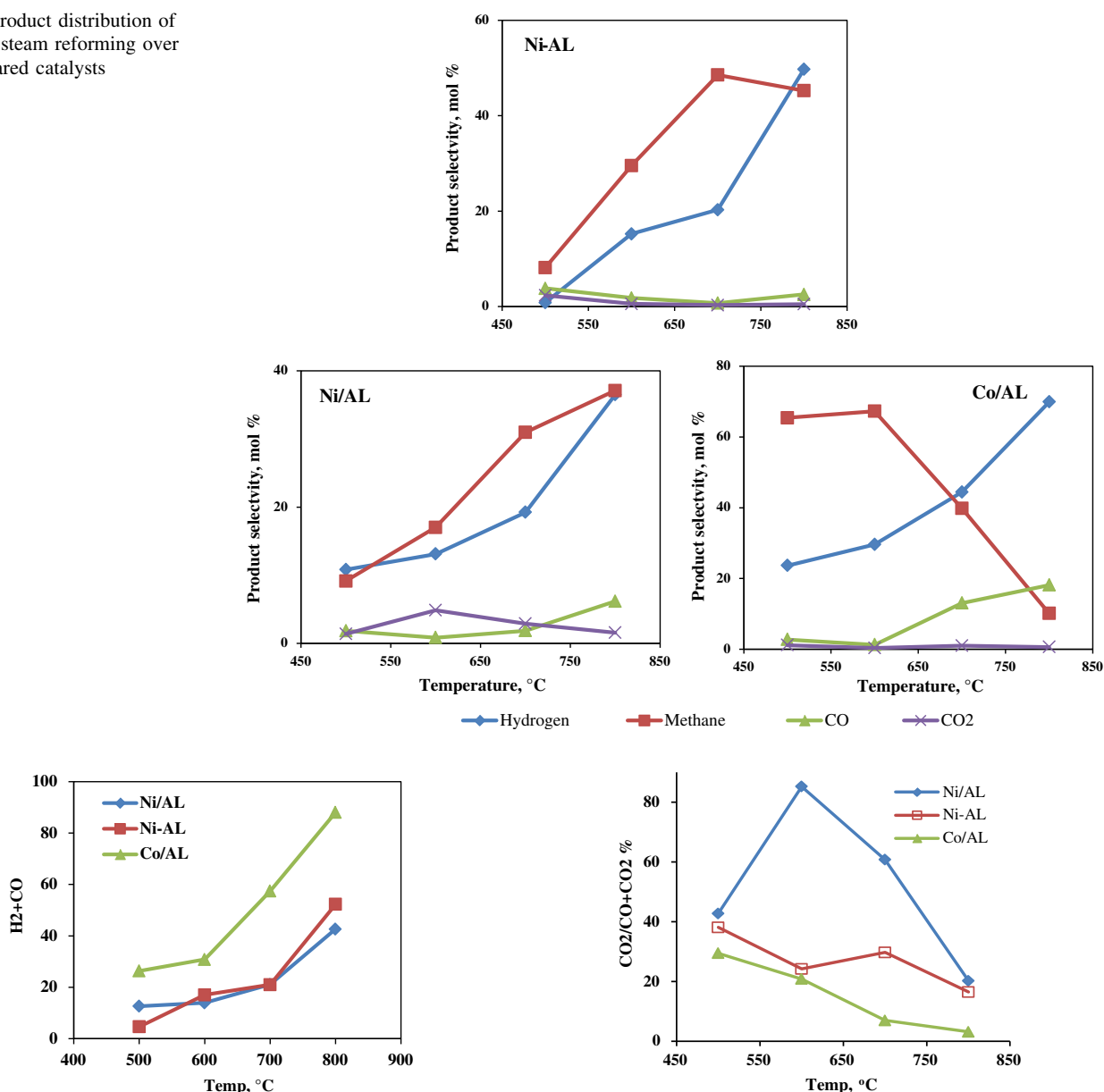


Fig. 9 H₂ + CO over the prepared catalysts

Fig. 11 Effect of reaction temperature on CO conversion (or WGSR)

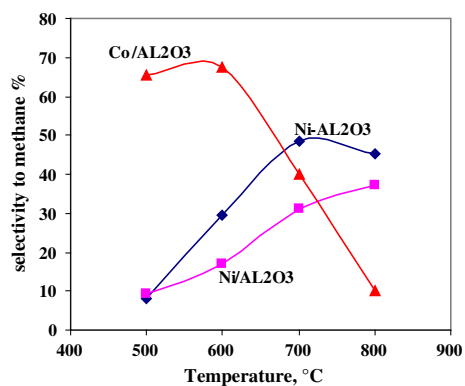


Fig. 10 Methane selectivity over the prepared catalysts

of CO₂ at higher temperature reflecting the CO₂ reforming of methane can take place over this catalyst (reaction 5) [31].

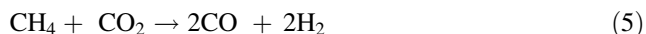
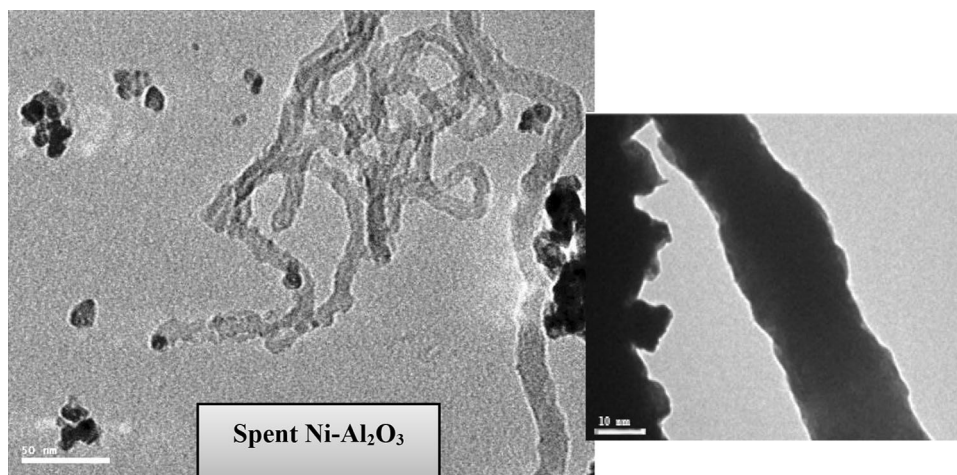


Figure 11 shows the CO₂/(CO + CO₂) ratio, which represents the CO conversion for the WGS reaction. All of the prepared catalysts favor WGS reaction at low reaction temperature. On the other hand, we can show that Ni catalysts favor WGS reaction more than that of Co catalyst. However, Ni/Al₂O₃ is a good GSR catalyst not only to produce H₂ by SR but also to decrease the CO ratio by WGS reaction. This also explains why Ni/Al₂O₃ catalyst

Fig. 12 TEM image of spent Ni–Al₂O₃ catalyst



shows high hydrogen yield at a lower temperature than Ni–Al₂O₃ catalyst.

From the practical application point of view, the use of gasoline as fuel in fuel cells needs high H₂ yield with very low amount of CO (<2 ppm). So, Co–Al₂O₃ catalyst can be used as a primary catalyst to produce high H₂ yield, while Ni/Al₂O₃ catalyst can be used as a secondary catalyst for conversion of CO to CO₂ and production of more hydrogen with low CO by WGS reaction.

Characterization of spent catalysts

Generally, the stability of any catalysts depends on the degree of metal sintering at high temperature and/or the carbon deposited behavior, which can block the active center leading to the decrease of catalytic activity. So, in this section we studied the characterization of the three catalysts after 10 h of GSR reaction.

High-resolution transmission electron microscopy

The three catalysts were analyzed by TEM to gain a deeper insight into the type of carbon deposited on the surface. TEM images for Ni/Al₂O₃, Ni–Al₂O₃ and Co/Al₂O₃ catalysts after 10 h of gasoline steam reforming reaction are presented in Fig. 12. The catalysts show coke formation with different morphologies. The image of Ni–Al₂O₃ reveals that the carbons are not an internal empty tube but opaque nano-rod. However, TEM images of the spent Ni/Al₂O₃ catalysts reveal the formation of amorphous carbon in addition to CNTs with Ni particles at the top of the tubes (indicated by the red circle in Fig. 13). In the case of Co/Al₂O₃ catalyst (Fig. 14), Web-like micrometer long CNTs partially covering the catalyst particle surface can be clearly observed. The figure also reveals the formation of carbon nano-fiber beside CNTs as confirmed by high oxidation temperature in thermal analysis data.

X-ray diffraction analysis

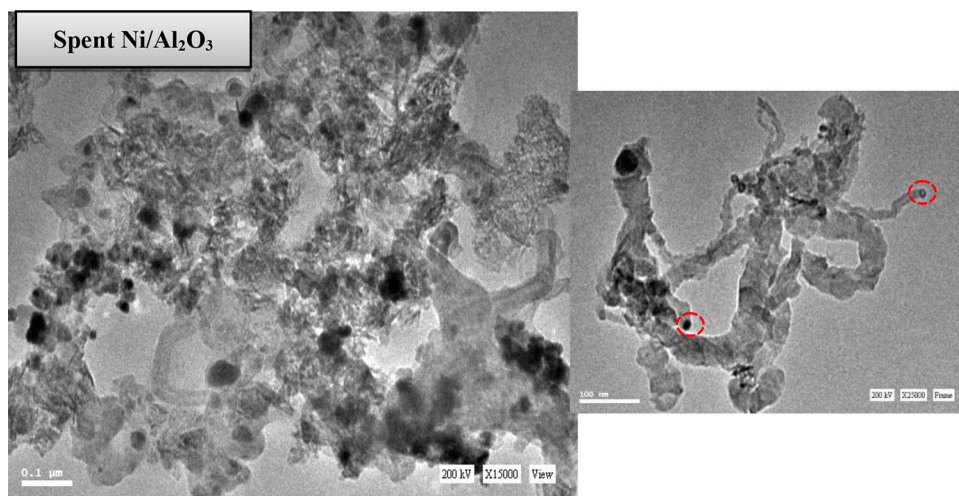
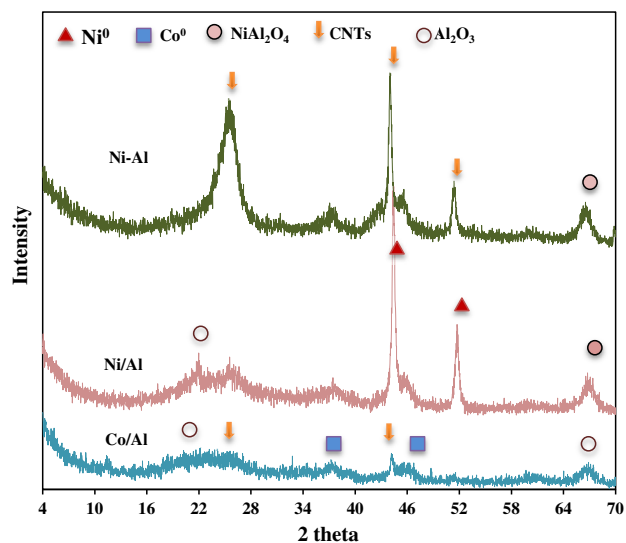
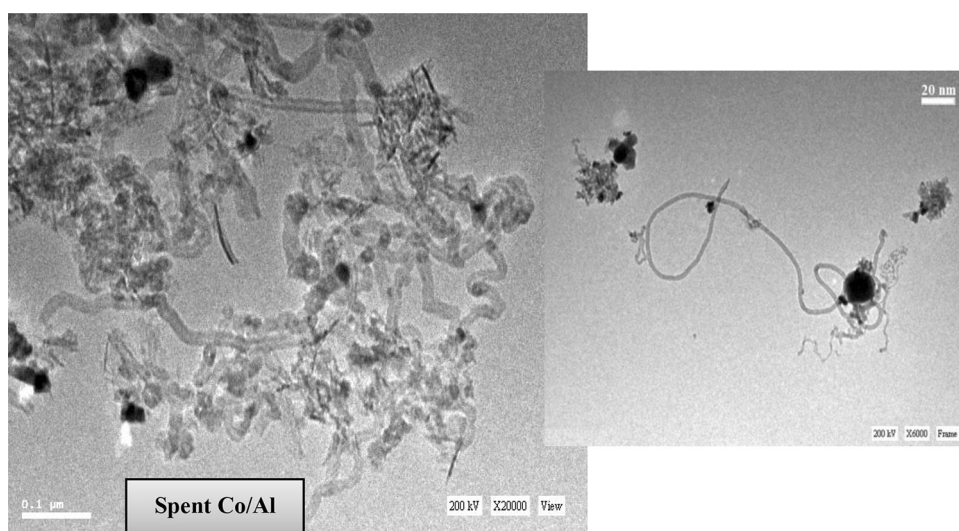
Figure 15 shows the XRD pattern of spent catalysts after gasoline steam reforming. Ni–Al₂O₃ catalyst shows strong peaks at $2\theta = 26.5^\circ$, 42.9° and 53.2° representing the (002), (100) and (004) graphitic basal plane reflection in the form of CNTs [ref. JCPDS card (00-058-1638)]; the peak assigned NiAl₂O₄ was also observed. It is worth noting that, although the catalyst was reduced before reaction there is not any peak assigned to the presence of Ni⁰ metal was observed due to the absence of free NiO in the fresh catalyst and the difficult reducibility of NiAl₂O₄ spinel under the reaction condition. Moreover, the graphite carbon phase is prominent compared to the peaks of Al₂O₃ support.

For Ni/Al₂O₃, NiAl₂O₄ was observed in addition to Ni⁰ (at 2θ reflections of 44.5° , 51.7°) and the peak attributed to NiO phase completely disappeared. The sharpness and high intensity of Ni⁰ peaks may be indicating that the Ni metal sintering is unavoidable for this catalyst under the reaction conditions.

On the other hand, the small intensity of all peaks in Co/Al₂O₃ catalyst may be attributed to the large amount of carbon deposited on the metal site and/or the pillaring formation.

Thermo-gravimetric analysis

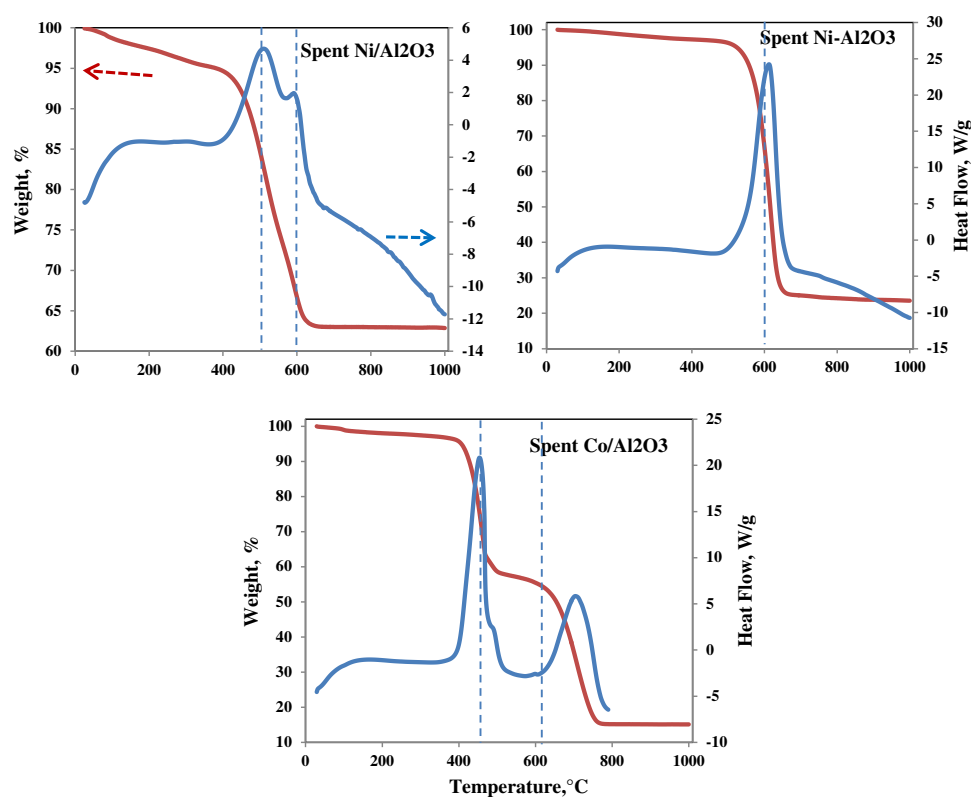
Table 3 shows the amount of carbon deposited per gram catalysts. Ni/Al₂O₃ catalyst seems to show a better resistance to coke formation, or promoting the gasification of the carbon formed on the catalyst surface, followed by Ni–Al₂O₃ and Co/Al₂O₃ catalysts. This result is greatly consistent with the catalytic activity toward CO₂ production, indicating that the current reactions (carbon gasification) primarily depend on the surface metal and also on the preparation methods.

Fig. 13 TEM image of spent Ni/Al₂O₃ catalyst**Fig. 14** TEM image of spent Co/Al₂O₃ catalyst**Fig. 15** XRD pattern for the spent catalysts**Table 3** The amount of carbon formed (g/g catalysts)

Catalysts	Weight loss (g/g catalysts)
Ni/Al ₂ O ₃	0.37
Ni–Al ₂ O ₃	0.76
Co/Al ₂ O ₃	0.85

As shown in Fig. 16, the three catalysts showed different behavior toward weight loss. A single-step degradation was observed over a Ni–Al₂O₃ catalyst at temperature above 600 °C indicating the deposition of carbon in the graphitic form [32, 33], while in case of Ni/Al₂O₃, most of carbon formed in the form of mono atomic carbon and filamentous coke (lower than 550 °C). The mono atomic carbon can be oxidized easy at low temperature, while the filamentous carbon is more stable and can be oxidized at higher temperatures [34]. This indicates that the

Fig. 16 TGA profile for nano- Al_2O_3 catalyst after 10 h gasoline steam reforming



preparation of $\text{Ni-Al}_2\text{O}_3$ by co-precipitation method enhances the graphitization degree of the deposit carbon.

However, in $\text{Co/Al}_2\text{O}_3$ catalyst, about 57.74 % of deposit carbon was in the form of mono atomic carbon and filamentous coke (lower than 550 °C). And 42.26 % of deposit carbon was carbon in the high graphitic form (higher than 600 °C), the higher oxidation temperature of this peak (700 °C) is due to the formation of carbon nano-fibers beside the CNTs [35], which is in a good agreement with the TEM data.

Raman of spent catalysts

Raman spectra for the three spent catalysts are shown in Fig. 17. All spectra had two bands: the first band is between 1,200 and 1,450 cm^{-1} (D-band) which is assigned to the disorder vibration of C–C bond [36], and the second band is between 1,500 and 1,700 cm^{-1} (G-band) assigned to the carbon material with sp^2 orbital structure [37]. The G-band is a graphitic band produced by the high degree of symmetry and order of these graphitic carbon materials; it provides information about the electronic properties of the filamentous carbon and is used to identify well-ordered CNTs [38, 39]. These findings suggest that the carbon species found on the surface of the catalysts tested in gasoline steam reforming consisted of deactivating (encapsulated carbon)

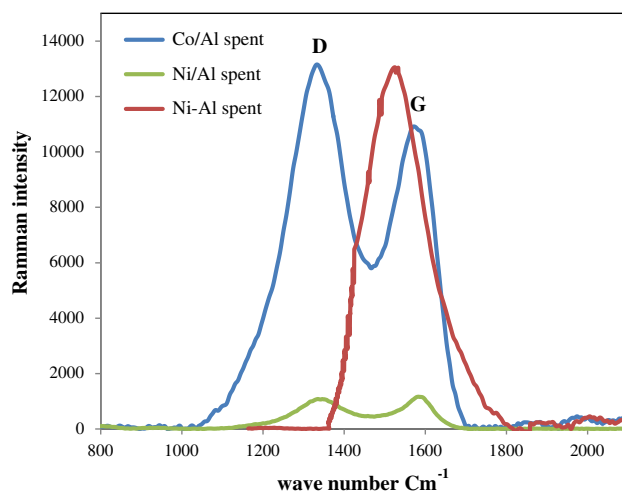


Fig. 17 Raman spectra of the spent catalysts

and non-deactivating carbon (whisker carbon) [36, 37], whose origins are diverse [40].

From Fig. 17 we can note that the intensities of the two bands were very high for $\text{Co/Al}_2\text{O}_3$ catalysts compared to $\text{Ni/Al}_2\text{O}_3$ one and that the intensity of the two bands was almost symmetric in $\text{Ni/Al}_2\text{O}_3$, which means that in case $\text{Ni/Al}_2\text{O}_3$ the carbon filaments was coexistent with amorphous carbon. In contrast, the high intensity of the D-band in $\text{Co/Al}_2\text{O}_3$ indicates that, this catalyst favors the formation of polymeric encapsulated carbon [26], which leads to

rapid deactivation. Moreover, the spectra of Ni–Al₂O₃ catalyst shows that, the intensity of G-band (between 1,400 and 1,700 cm⁻¹) is very high with respect to that of D-band (which may be neglected) indicating the deposition of carbon in the graphitic form as suggested by TGA and TEM data.

Conclusion

In this work, we prepare three different nano-alumina catalysts; the first two catalysts are nickel alumina catalysts prepared by two different methods (co-precipitation and impregnation method); the third catalyst was Co/Al₂O₃ prepared by impregnation method to study the effect of metal type on the performance of the prepared catalysts. It was found that Co/Al₂O₃ shows the most reactivity toward hydrogen production from GSR reaction (highest activity and highest H₂/CO ratio). Moreover, Ni–Al₂O₃ catalyst exhibited promising properties in gasoline steam reforming reaction than Ni/Al₂O₃. This may be attributed to small particle sizes, high surface area, and strong metal–support interaction of the catalyst prepared by the co-precipitation method.

On the other hand, the characteristic properties of the three catalysts after 10 h of GSR shows that graphitic carbon was formed on the surface of the Ni–Al₂O₃ catalyst, and the amorphous one covered most of the surface of the Ni/Al₂O₃ catalyst. Although the formation of NiAl₂O₄ plays an important role in decreasing the sintering process, it increases the graphitization degree of carbon deposit. However, over Co/Al₂O₃ catalyst the major amount of carbon was in the form of mono atomic carbon and filamentous coke and the small amount was graphitic carbon in the form of carbon nano-fibers beside the CNTs.

Open Access This article is distributed under the terms of the Creative Commons Attribution License which permits any use, distribution, and reproduction in any medium, provided the original author(s) and the source are credited.

References

- Cheekatamarla, P.K., Lane, A.M.: Efficient bimetallic catalysts for hydrogen generation from diesel fuel. *Int. J. Hydrog. Energy* **30**, 1277 (2005)
- Hoang, D.L., Chan, S.H.: Modeling of a catalytic autothermal methane reformer for fuel cell application. *Appl. Catal. A* **268**, 207 (2004)
- Simson, A., Farrauto, R., Castaldi, M.: Steam reforming of ethanol/gasoline mixtures: Deactivation, regeneration and stable performance. *Appl. Catal. B* **106**, 295 (2011)
- Villegas, L., Guillaume, N., Provendier, H., Daniel, C., Masset, F., Mirodatos, C.: A combined thermodynamic/experimental study for the optimisation of hydrogen production by catalytic reforming of isooctane. *Appl. Catal. A* **281**, 75 (2005)
- Roy, B., Martinez, U., Loganathan, K., Datye, A.K., Leclerc, C.A.: Effect of preparation methods on the performance of Ni/Al₂O₃ catalysts for aqueous-phase reforming of ethanol: part I-catalytic activity. *Int. J. Hydrog. Energy* **37**, 8143–8153 (2012)
- Gaur, S., Haynes, D.J., Spivey, J.J.: Rh, Ni, and Ca substituted pyrochlore catalysts for dry reforming of methane. *Appl. Catal. A* **403**, 142 (2011)
- Gamba, O., Moreno, S., Molina, R.: Catalytic performance of NiePr supported on delaminated clay in the dry reforming of methane. *Int. J. Hydrog. Energy* **36**, 1540 (2011)
- Sinfelt, J.H., Yates, D.J.C.: Catalytic hydrogenolysis of ethane over the noble metals of Group VIII. *J. Catal.* **8**, 82–90 (1967)
- Grenoble, D.C., Estadt, M.M., Ollis, D.F.: The chemistry and catalysis of the water gas shift reaction: 1. The kinetics over supported metal catalysts. *J. Catal.* **67**, 90–102 (1981)
- Vannice, M.A.: The catalytic synthesis of hydrocarbons from H₂CO mixtures over the Group VIII metals: V. The catalytic behavior of silica-supported metals. *J. Catal.* **50**, 228 (1977)
- Therdthianwong, S., Therdthianwong, A., Siangchin, C., Yongprapat, S.: Synthesis gas production from dry reforming of methane over Ni/Al₂O₃ stabilized by ZrO₂. *Int. J. Hydrog. Energy* **33**, 991 (2008)
- Garbarino, G., Campodonico, S., Perez, A.R., Carnasciali, M.M., Riani, P., Finocchio, E., Busca, G.: Spectroscopic characterization of Ni/Al₂O₃ catalytic materials for the steam reforming of renewables. *Appl. Catal. A* **452**, 163 (2013)
- Takanabe, K., Aika, K., Inazu, K., Baba, T., Seshan, K., Lefferts, L.: Steam reforming of acetic acid as a biomass derived oxygenate: bi-functional pathway for hydrogen formation over Pt/ZrO₂ catalysts. *J. Catal.* **243**, 263 (2006)
- Delacruz, V.M.G., Guez, R.P., Ternero, F., Holgado, J.P., Caballero, A.: Preparation of hydrogen and carbon nanotubes over cobalt-containing catalysts via catalytic decomposition of ethanol. *J. Phys. Chem. C* **116**, 2919 (2012)
- Alonso, D.S.J., Juan, J.J., Gomez, M.J.I., Martinez, M.C.R.: Ni, Co and bimetallic Ni–Co catalysts for the dry reforming of methane. *Appl. Catal. A* **371**, 54 (2009)
- Parida, K.M., Pradhan, A.C., Das, J., Sahu, N.: Synthesis and characterization of nano-sized porous gamma-alumina by control precipitation method. *Mater. Chem. Phys.* **113**, 244 (2009)
- Ebiad, M.A., Abd El-Hafiz, D.R., Elsalamony, R.A., Mohamed, L.S.: Ni supported high surface area CeO₂–ZrO₂ catalysts for hydrogen production. *RSC Adv.* **2**, 8145 (2012)
- Xi-kun, G., Ping-ping, X., Shu-dong, L.: Preparation of Cu/La₂O₃–ZrO₂–Al₂O₃ catalyst and its catalytic properties for selective reduction of NO. *J. Fuel Chem. Technol.* **36**, 732 (2008)
- Hao, Z., Zhu, Q., Jiang, Z., Hou, B., Li, H.: Characterization of aerogel Ni/Al₂O₃ catalysts and investigation on their stability for CH₄–CO₂ reforming in a fluidized bed. *Fuel Process. Technol.* **90**, 113 (2009)
- Padilla, R., Benito, M., Rodriguez, L., Serrano, A., Munoz, G., Daza, L.: Nickel and cobalt as active phase on supported zirconia catalysts for bio-ethanol reforming: Influence of the reaction mechanism on catalysts performance. *Int. J. Hydrog. Energy* **35**, 8921 (2010)
- Batista, M.S., Santos, R.K.S., Assaf, E.M., Assaf, J.M., Ticianelli, E.A.: High efficiency steam reforming of ethanol by cobalt-based catalysts. *J. Power Sour.* **134**, 27 (2004)
- Seo, J.G., Youn, M.H., Song, I.K.: Hydrogen production by steam reforming of liquefied natural gas (LNG) over nickel catalyst supported on mesoporous alumina prepared by a non-ionic surfactant-templating method. *Int. J. Hydrog. Energy* **34**, 1809 (2009)

23. Chen, J.X., Wang, R.J., Zhang, J.Y., He, F., Han, S.: Effects of preparation methods on properties of Ni/CeO₂-Al₂O₃ catalysts for methane reforming with carbon dioxide. *J. Mol. Catal. A Chem.* **235**, 302 (2005)
24. Kwak, S.B., Kim, J., Kang, M.: Hydrogen production from ethanol steam reforming over core-shell structured Ni_xO_y, Fe_xO_y, and Co_xO_y-Pd catalysts. *Int. J. Hydrog. Energy* **35**, 11843 (2010)
25. Zhou, Y., Guo, Q., Zhang, M., Yagi, J., Hatakeyama, L.H., Chen, J., Sakurai, M., Kameyama, H.: A novel catalyst with plate-type anodic alumina supports, Ni/NiAl₂O₄/g-Al₂O₃/alloy, for steam reforming of methane. *Appl. Catal. A* **347**, 200 (2008)
26. de Sousa, F.F., de Sousa, H.S.A., Oliveira, A.C., Junior, M.C.C., Ayala, A.P., Barros, E.B., Viana, B.C., Filho, J.M., Oliveira, A.C.: Nanostructured Ni-containing spinel oxides for the dry reforming of methane: effect of the presence of cobalt and nickel on the deactivation behaviour of catalysts. *Int. J. Hydrog. Energy* **37**, 3201 (2012)
27. Jacobs, G., Chaney, J.A., Patterson, P.M., Das, T.K., Davis, B.H.: Fischer-Tropsch synthesis: study of the promotion of Re on the reduction property of Co/Al₂O₃ catalysts by in situ EXAFS/XANES of Co K and Re LIII edges and XPS. *Appl. Catal. A* **264**, 203 (2004)
28. Jacobs, G., Davis, B.H.: Low temperature water-gas shift: applications of a modified SSITKA-DRIFTS method under conditions of H₂ co-feeding over metal/ceria and related oxides. *Appl. Catal. A* **333**, 192 (2007)
29. Akande, A.J., Idem, R.O., Dalai, A.K.: Synthesis, characterization and performance evaluation Ni/Al₂O₃ catalysts for reforming of crude ethanol for hydrogen production. *Appl. Catal. A* **287**, 159 (2005)
30. Rabe, S., Vogel, F., Truong, T.B., Shimazu, T., Wakasugi, T., Aoki, H., Sobukawa, H.: Catalytic reforming of gasoline to hydrogen: kinetic investigation of deactivation processes. *Int. J. Hydrog. Energy* **34**, 8023 (2009)
31. Ferencz, Zs, Baán, K., Oszkó, A., Kónya, Z., Kecskés, T., Erdohelyi, A.: Dry reforming of CH₄ on Rh doped Co/Al₂O₃ catalysts. *Catal. Today* **228**, 123–130 (2014)
32. Zhang, L., Li, W., Liu, J., Guo, C., Wang, Y., Zhang, J.: Ethanol steam reforming reactions over Al₂O₃SiO₂-supported Ni-La catalysts. *Fuel* **88**, 511 (2009)
33. Freni, S., Carvillaro, S., Mondello, N., Spadaro, L., Frusteri, F.: Production of hydrogen for MC fuel cell by steam reforming of ethanol over MgO supported Ni and Co catalysts. *Catal. Commun.* **4**, 259 (2003)
34. Wang, P., Tanabe, E., Ito, K., Jia, J., Morioka, H., Shishido, T., et al.: Filamentous carbon prepared by the catalytic pyrolysis of CH₄ on Ni/SiO₂. *Appl. Catal. A* **231**, 35 (2002)
35. Awadallah, A.E., Aboul-Enein, A.A., Aboul-Gheit, A.K.: Various nickel doping in commercial NiMo/Al₂O₃ as catalysts for natural gas decomposition to CO_x-free hydrogen production. *Renew. Energy* **57**, 671 (2013)
36. Pinheiro, A.L., Pinheiro, A.N., Valentini, A., Filho, J.M., Sousa, F.F., Sousa, J.R., Rocha, M.G.C., Bargiela, P., Oliveira, A.C.: Analysis of coke deposition and study of the structural features of MAI₂O₄ catalysts for the dry reforming of methane. *Catal. Commun.* **11**, 11 (2009)
37. Damyanova, S., Pawelec, B., Arishtirova, K., Martinez Huerta, M.V., Fierro, J.L.G.: The effect of CeO₂ on the surface and catalytic properties of Pt/CeO₂-ZrO₂ catalysts for methane dry reforming. *Appl. Catal. B* **89**, 149 (2009)
38. Dresselhaus, M.S., Dresselhaus, G., Jorio, A., Souza Filho, A.G., Saito, R.: Raman spectroscopy on isolated single wall carbon nanotubes. *Carbon* **40**, 2043 (2002)
39. Pan, C., Bao, Q.: Well-aligned carbon nanotubes from ethanol flames. *J. Mater. Sci. Lett.* **21**, 1927 (2002)
40. Amin, A.M., Croiset, E., Epling, W.: Review of methane catalytic cracking for hydrogen production vol 3. *Int. J. Hydrog. Energy* **36**, 2904 (2011)